Controller Design for a High Precision Elastically Supported Hybrid Active Magnetic Guidance

Mirko Büchsenschütz
Ilmenau University Of Technology
Ilmenau, Thuringia, Germany
mirko.buechsenschuetz@tu-ilmenau.de

Thomas Sattel
Ilmenau University Of Technology
Ilmenau, Thuringia, Germany
thomas.sattel@tu-ilmenau.de

Abstract

The design of multi coordinate drives (MCD) with nanometre positioning uncertainty and long planar motion range of several hundred millimetres is a worldwide research challenge. Active magnetic guidance (AMG) is suitable for these precision applications due to its non-contact support principle. One drawback is the heat generation due to ohmic loss in the control coil which should be minimized and kept constant to meet high precision demands [1, pp. 83-84].

In [2] an elastically supported hybrid active magnetic guidance (ES-HAMG) is proposed. A hybrid magnet combines a permanent magnet with a coil, additionally it is connected in series with a mechanical spring. This device is capable of reducing the thermal dissipation by 80% at varying load force on a sample ES-HAMG.

This contribution gives a more comprehensive view on ES-HAMG in MCD than [2]. A model to estimate possible savings in power dissipation is derived in detail. The employed controller design theory is given. Experiments confirm theoretical energy savings and the nanopositioning capabilities.

1 Introduction

Multi coordinate drives (MCD) that are suitable for sub micrometre positioning in a large range of motion (stroke) are used in several industries, especially semiconductor manufacturing. Today, these systems are mostly guided by air bearings which are not fully suitable to vacuum conditions. Active magnetic guidance (AMG) could overcome this disadvantage, moreover it acts as a contactless guiding and positioning element [3]. One drawback of AMG is the heat generation due to ohmic losses of the control coil. In high precision systems, all heat sources have to be reduced, kept constant or captured to prevent the thermal flow from spreading into the structures, especially the metrology frame.

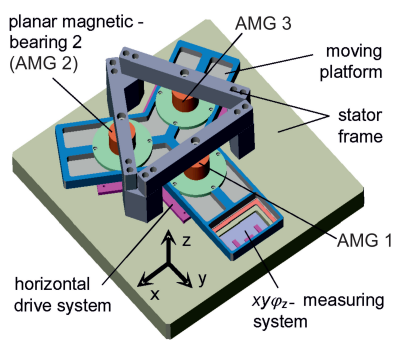

Figure 1: ZKA4 MCD [3], [4]

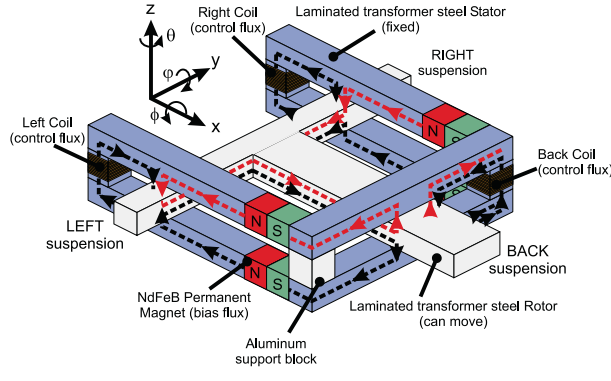

Figure 2: TU-Module [5]

Figure 1 and 2 show two sample designs of magnetically guided MCD. The moving platform (slider) of the ZKA4 [3] is magnetically levitated by the reluctance forces of three electromagnets (AMG 1 to AMG 3). Three laser interferometers (not shown) provide sufficient resolution in vertical direction. The horizontal drive and measuring system allows long range precise positioning. The system offers a full stroke of 30 x 30 x 0.2 mm^3. The TU-Module's [5] rotor is levitated by reluctance forces as well, furthermore it exerts bidirectional forces. It offers a XY stroke of 160 x 160 mm^2. By positioning the slider, the load forces of both systems vary due to relative translation of the slider's centre of gravity. Today, both systems do not have sufficient stroke, as wafers offer diameters about 300 mm and future wafers will have 450 mm in diameter.

Increasing the stroke goes along with a significant raise of the slider's mass and load deviations, the AMG has to compensate for. In hybrid AMG (HAMG) where permanent magnets are combined with coils, the static equilibrium of a specific load is given at zero power dissipation, if the amount of current to stabilize magnetic levitation is neglected. However, the load deviations during positioning have to be compensated by current offsets in larger quantities.

Several techniques exist to manipulate magnetic flux and thus the magnetic force, with virtually no heat generation. All alternatives, known to the authors, make use of an additional actuator to exert motion or stress within the magnetic circuit. In [6] magnetostrictive material has been loaded by a controlled piezoelectric element to vary the magnetic flux in a magnetic levitation system to approach zero power at varying load and constant position of the levitated object. The stabilization has been performed by a parallel control coil. Other techniques are based on rotation [7] or translation [8] of permanent magnets within the magnetic flux path. In [9] several magnetic circuits are presented, which are capable of varying the flux path reluctance which can be used to directly manipulate the working flux or to branch off magnetic flux to a an alternative path. This is performed by active positioning of iron material. In [10] a whole hybrid magnet is elastically suspendeded, which leads to an additional motion of the actuator depending on the spring constant and the actual load during operation. In this case the working gap corresponds addtionally to a variable reluctance element, where the spring constant and initial load determine the reluctance depending on the magnetic force in steady state. Furthermore this technique is reffered to as elastically supported hybrid active magnetic guidance (ES-HAMG). It has been applied to active vibration isolation [10] which is essential for high precision positioning applications. Thus there is a chance to combine guidance of planar (lateral) movement and vibration isolation within a single low power electromagnetic system. In [2], nanopositioning capabilities and possible energy savings of ES-HAMG have been demonstrated. It is subject to this contribution to give a more detailed view on the system and the controller design, which has been applied in a high precision AMG before [11].

2 Working Principle

Zero power controlled HAMG behaves as if it has a negative stiffness [10]. Generally, by connecting two springs with spring constants c and c_M in series the resulting stiffnes c_r is

$$c_r = \frac{c\,c_M}{c + c_M}. \tag{1}$$

If one of the springs has a negative stiffness, (1) can satisfy $|c_r| = \infty$ with

$$c = -c_M. \tag{2}$$

Thus, infinite stiffnes can be achieved by connecting a mechanical spring (c) in series with a negative magnetic spring (c_M), theoretically. Practically it is impossible to satisfy (2) exactly, furthermore

c_M is not constant due to its nonlinear and hysteretic magnetic characteristics. In the dynamic case, we cannot assume (1), as the magnetic stiffnes requires a magnet's intermediate mass m_M between both springs. As heat transfer is a relatively slow process in macro systems, the steady state power dissipation is of importance. Sections 3.5 and 5.2 show that it is possible to obtain high stiffnes and significant savings in the amount of power dissipation even with a linear mechanical spring.

Fig. 3 shows a MCD where the slider is guided by two ES-HAMG, pictured as spring, damper and a hybrid magnet. As the center of gravity (CG) is displaced, the right hybrid magnet exerts a higher guidance force $F_{M,2}$ than the left one, wich leads to higher strain of the right mechanical spring.

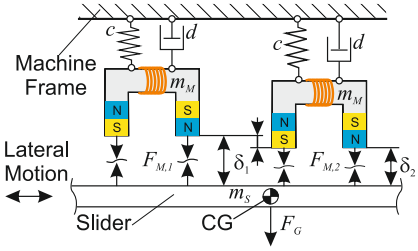

Figure 3: Schematic view of MCD with ES-HAMG (2D) [2]

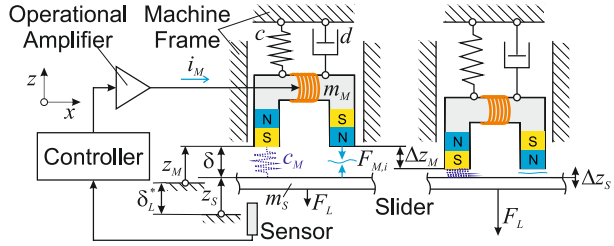

Figure 4: a) Principle of ES-HAMG (left) , b) ES-HAMG after load deviation (right) [2]

As a common principle in controller design for AMG, the magnetic force F_M is linearized in the intended point of operation with respect to the armatures position and the current to force factor [12, p. 31]. Thus the magnetic force can be represented as a magnetic spring c_M in parallel with an actuation force $F_{M,i}$ that goes along with an electric current (Figure 4).To manipulate the force $F_{M,i}$, sensor, controller and operational amplifier are standard components in AMG to provide the appropriate actuating current i_M (Figure 4a). A load deviation ΔF_L leads to a position deviation Δz_S, thus the control equipment counteracts by increasing $F_{M,i}$. The load deviation is forwarded to the mechanical spring which causes a dislocation Δz_M (Fig. 4b), reducing the working gap δ. According to the negative stiffness c_M, the force portion of the magnetic spring $F_{M,c}$ (not shown) increasess, leading the control equipment to decrease $F_{M,i}$, thus saving power dissipation.

The presented ES-HAMG control structure differs from zero power control, as there is no current integral feedback. This leads to infinite stiffness at the cost of a slight amount of power dissipation instead of approaching zero power at the cost of almost infinite stiffness. This choice is essential to achieve high precision positioning.

3 Modeling

This section provides a physical models of ES-HAMG to estimate energy savings and spring constants before controller design. At first, 3.1 gives an overview on modelling assumptions for the engaged technical domains. Sections 3.2 and 3.3 explain all basic equations for subsequent derivations in sections 3.4 and 3.5. ES-HAMG is suitable for applications with varying load and a mainly constant control input of the reluctance actuator. Based on the mean load F_L^*, the appropriate working gap and the corresponding spring constant is derived in 3.4. The theoretical power dissipation of ES-HAMG in comparison to pure HAMG is subject to 3.5.

3.1 Assumptions

In the design process of magnetic actuators, four technical domains and their couplings have to be considered [13, p. 58]. Figure 5 shows all domains to be considered for ES-HAMG systems. Inter-domain couplings are represented as gray arrows.

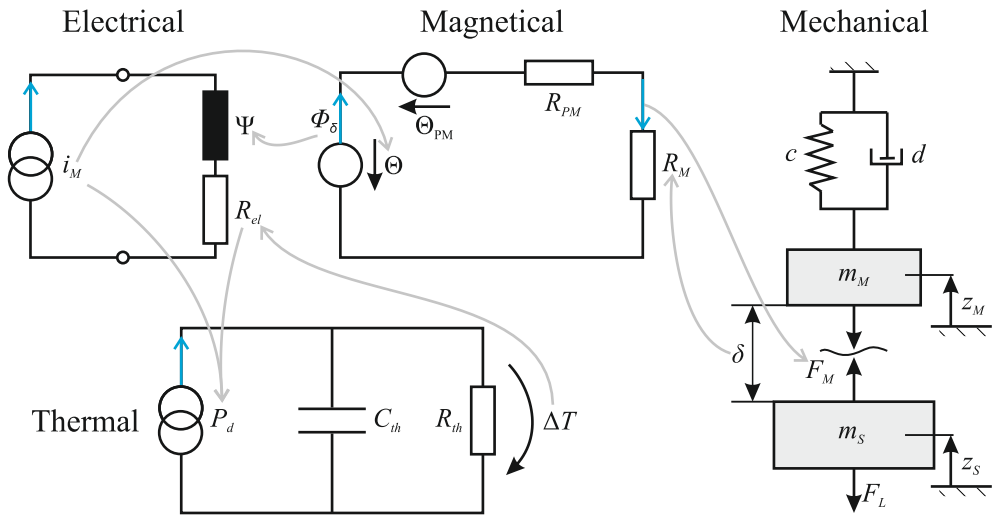

Figure 5: Electro-magneto-mechanical energy conversion and thermal dissipation ([13, p. 58])

The electric domain is considered to be a variable current source (actuation variable) i_M that perfectly compensates for the induced voltage $-\partial\Psi/\partial t$ and the ohmic resistance of the coil R. Practically, the phase lag of the current source may be measured and compensated for.

A magnetic circuit of a hybrid magnet with serial flux path is assumed, eddy current effects are neglected. Θ and Θ_{PM} are magnetomotive forces of the control coil and the permanent magnet (PM). R_{PM} is the constant reluctance of the PM, R_M depends on δ as it represents the variable reluctance of the working gap. ϕ_δ is the magnetic flux, leading to the force F_M. This simple network model does not consider stray flux, magnetic saturation or hysteresis but suffices to estimate the system behaviour.

The mechanical domain is depicted as a lumped mass model of the ES-HAMG (compare to Figure 4). Spring and damper (constants: c, d) represent the elastic support of the hybrid magnet. The upper mass m_M is the moving mass of the hybrid magnet and additional moving structures to ensure guidance in one DOF. The magnetic force F_M acts on both moving masses, where m_S is the intended target mass, as it represents the slider and its armature. The load force F_L is supposed to be time dependent.

The termal circuit is not necessary to model energy conversion in the electrical domain if we can assume a high thermal capacity C_{th} [13, p. 58]. Nevertheless it is depicted to demonstrate the thermal coupling to the electric circuit. Thermal resistances R_{th} that are passed by thermal current generate temperature differences ΔT which have to be kept low and/or constant. Larger thermal networks are necessary to model whole machine structures to consider thermal isolation and thermal current pathes. The strategy of ES-HAMG is to minimize the termal current source P_d, as it reduces the thermal design effort in precision machines [1, p. 84].

3.2 Balance laws

This section deals with the balance equations, considered for each technical domain in section3.1. Equation (3)

$$U = R\,i_M + \frac{\partial \Psi}{\partial t} \tag{3}$$

is the electric balance equation of a simple electric circuit, including a coil. As i_M is assumed to be the actuation variable, it is reasonable to calculate the maximum Voltage U at the intended operation mode. The balance equation of the magnetic circuit is

$$\Theta + \Theta_{PM} = (R_{PM} + R_M)\phi_\delta. \tag{4}$$

Mechanical force balance for each moving mass is considered, according to figure 5 and slight damping d_S of the slider , in equations (5) and (6)

$$m_M\,\ddot{z}_M + d\,\dot{z}_M + c\,z_M = -F_M \tag{5}$$

$$m_S\,\ddot{z}_S + d_S\,\dot{z}_S = F_M - F_L. \tag{6}$$

3.3 Component laws

The ohmic resistance of the control coil is [13, p. 19]

$$R_{el} = w^2 \frac{\rho\, l_m}{k_{Cu} A_w}, \tag{7}$$

where k_{Cu} is the copper filling factor, A_w the cross section of the coil, ρ the specific resistance of the coil material and l_m the average winding length. It also realizes the magnetic coupling according to [13, p. 10]

$$\Theta = w\,i_M \tag{8}$$

and the power dissipation, which equals the thermal current source [13, p. 58]

$$P_d = R_{el}\,i_M^2. \tag{9}$$

The thermal influence on the ohmic resistance of the control coil is neglected in (7).

The magnetic reluctance of a simple geometry is [13, p. 15]

$$R_{mag} = \frac{l}{\mu A} \tag{10}$$

where l is the length of the flux line, A the cross section of the flux path and μ is the magnetic permeability of the material. According to (10), the reluctance of the permanent magnet is

$$R_{PM} = \frac{l_{PM}}{\mu_0 A_\delta} \tag{11}$$

and the variable reluctance of two working gaps is

$$R_M(\delta) = \frac{2\delta}{\mu_0 A_\delta}. \tag{12}$$

The attractive force of the hybrid magnet directly depends on the magnetic flux in two working gaps according to [13, p. 64]

$$F_M(\phi_\delta) = \frac{\phi_\delta^2}{\mu_0 A_\delta}. \tag{13}$$

The kinematic coupling of the working gap δ with both coordinates of the moving masses leads to additional coupling from the mechanic to the magnetic domain according to figure 4 we get

$$\delta = \delta_L^* + z_M - z_S. \tag{14}$$

3.4 Magnetostatic derivation of the appropriate spring constant

At first we consider the magnetic flux in both working gaps, from (8) and (4) we get

$$\phi_\delta(i_M, R_M) = \frac{w i_M + \Theta_{PM}}{R_M + R_{PM}}. \tag{15}$$

With (15), (11) and (12), ϕ_δ depends on the working gap and the actuating current

$$\phi_\delta(i_M, \delta) = \frac{(w i_M + \Theta_{PM}) A_\delta \mu_0}{l_{PM} + 2\delta}. \tag{16}$$

Remaining time invariant variables from the magnetic domain are eliminated with (16) and (13) to the magnetic force

$$F_M(i_M, \delta) = \frac{(w i_M + \Theta_{PM})^2 A_\delta \mu_0}{(l_{PM} + 2\delta)^2}. \tag{17}$$

We intend to have zero power dissipation $P_d = 0$, thus from (9) we assume $i_M = 0$ at the point of operation. Furthermore, the ES-HAMG has to compensate for a desired load $F_M = F_L^*$. From (17) we solve for the initial working gap δ_L^*,

$$F_M(0, \delta_L^*) = F_L^* \Leftrightarrow \delta_L^*(F_L^*) = \frac{\Theta_{PM}\sqrt{A_\delta \mu_0}}{F_L^*} + \frac{l_{PM}}{2}. \tag{18}$$

A mechanical spring constant is the derivative of the force with respect to its location. As the magnets force characteristic is nonlinear, the magnetic stiffness at zero current depends on the working gap,

$$c_M(0, \delta) = \frac{\partial F_M(0, \delta)}{\partial \delta} = -\frac{4\Theta_{PM}^2 A_\delta \mu_0}{(l_{PM} + 2\delta)^3}. \tag{19}$$

With (2),(18) and (19) we can solve for the appropriate mechanical spring constant, assuming a given hybrid magnet and a given load,

$$c(F_L^*) = -c_M(0, \delta_L^*) = \frac{4F_L^*\sqrt{F_L^*}}{\Theta_{PM}\sqrt{A_\delta \mu_0}}. \tag{20}$$

Equation (20) is sufficient to estimate the appropriate mechanical spring constant. To satisfy the intended vibration characteristics, a specific stiffnes c might be adjusted with the main parameters Θ_{PM} and A_δ.

3.5 Steady state power dissipation

ES-HAMG is beneficial, if the load varies continuosly as in planar positioning. Possible savings can be estimated with the results from 3.4 and some basic equations.

If inertia and damping forces are neglected in (5) and (6), we can solve for the steady state position of the hybrid magnet

$$z_{M,steady} = -\frac{F_L}{c}. \tag{21}$$

If we assume z_S to be constant, with (14) and (21) we get

$$\delta_{steady} = \delta_L^* - \frac{F_L}{c} - z_{S,steady}. \tag{22}$$

With (7), (9), (17), (18), (20) and (22) we get the steady state power dissipation as a function of the load force $p_d(F_L)$.

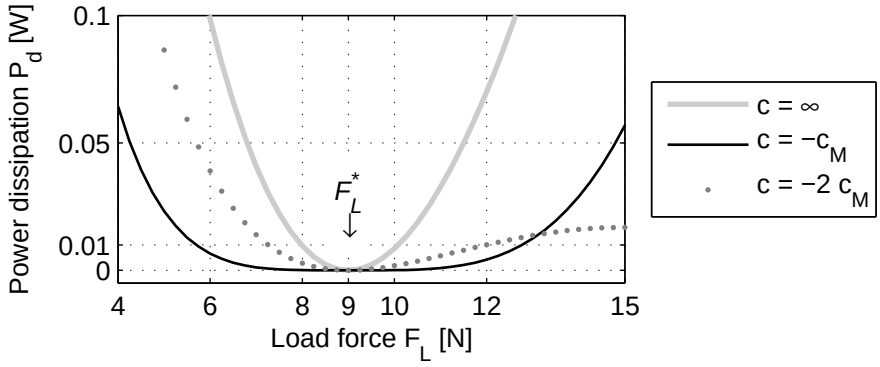

Figure 6: Calculated power dissipation $P_{d,steady}$ [W] in a load range for a varying mechanical stiffnes and a constant position of the levitated object ($z_{S,steady} = 0$)

Figure 6 compares different evaluations of $P_{d,steady}$ for a given load range from 4 N to 15 N with respect to the mechanical spring constant c. The parameters of the hybrid magnet approximately correspond to the test bench, described in section 5.1 ($c_M \approx -40\,\frac{\mathrm{N}}{\mathrm{mm}}$, $F_L^* \approx 9\,\mathrm{N}$, $\delta_L^* \approx 241\,\mu\mathrm{m}$). At infinite stiffness c (HAMG), $P_{d,steady}$ osculates zero power at a single point of operation $F_L = F_L^* = 9\,\mathrm{N}$. If the load is altered, the power dissipation increases significantly. At $c = -cM$ (as intended in (2)), zero power is present at the same point of operation, in contrast the power dissipation within the load range is significantly lower.

The change in power dissipation $\partial P_{d,steady}/\partial F_L$ equals zero, where the electric current i_M changes its sign, or where the mechanical stiffnes complies with (2). With higher stiffness ($c = -2c_M$), $P_{d,steady}$ is higher in the range from 6 N to 12 N. A local maximum occurs at $F_L \approx 15\,\mathrm{N}$, as the absolute magnetic stiffness complies with the mechanical spring at this point of operation, as δ varies (22) and c_M depends on δ (19).

Figure 7 shows the same diagram as figure 6 for $c = -c_M$ with different positions of the slider ($z_{S,steady}$). $z_{S,steady} = 0$ has been discussed before. If there is a slightly smaller working gap δ ($z_{S,steady} = 20\,\mu\mathrm{m}$), no working point exists, where the ES-HAMG approaches zero power, as an external current is needed to weaken the PM's magnetomotive force in the whole range. Accordingly, at $z_{S,steady} = -20\,\mu\mathrm{m}$, external current is needed to support the PM around F_L^*. There exist

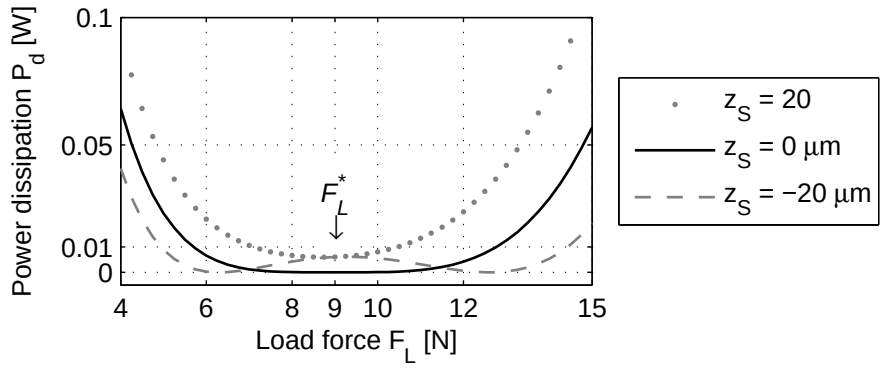

Figure 7: Calculated power dissipation $P_{d,steady}$ [W] in a load range for a constant mechanical stiffnes ($c = -c_M$) and different positions of the levitated object $z_{S,steady}$

two osculation points at approximately 6.25 N and 12.5 N where the external current switches its sign. This is a beneficial configuration, as it extends the load range of low power dissipation.

These exemplary evaluations show, that it is possible to decrease the dissipated heat by 90 % in the load range from 6 N to 12 N in theory. However, practically there are effects like hysteresis and an additional amount of power to stabilize magnetic levitation as examined experimentally in section 5.2.

4 Controller Design

Nanometre-precision positioning with an AMG has been presented in [11] based on PI state space control. The control structure is introduced in section 4.1, section 4.2 shows the pole placement procedure to find the appropriate controller gains.

4.1 Control Structure

Figure 8 shows a schematic of the top-level control structure. The control input $\mathrm{w}(t)$ is equivalent

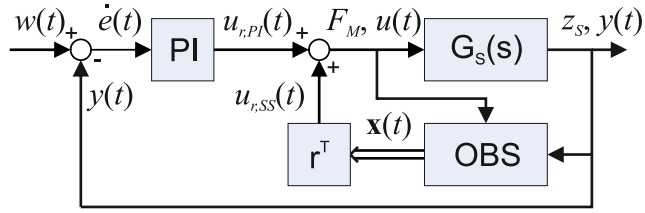

Figure 8: PI state space control structure [11]

to the desired position of the slider. The state vector $\mathbf{x}(t)$ contains the sliders position z_S and other variables. Only z_S is measured directly, thus $\mathbf{x}(\mathbf{t})$ is evaluated by the observer **OBS**. $G_S(s)$ denotes the mechanical transfer function of the plant. The controller consists of the state feedback $\mathbf{r}^\top$ and an additional **PI** controller. The actuating variable $u(t)$ is the magnetic force F_M. It has to be set with an inverse characteristic curve $i_M\left(F_{M,des}, \delta\right)$ that suffices $F_M\left(i_M\left(F_{M,des}, \delta\right), \delta\right) = F_{M,des}$.

The full system state of an ES-HAMG can be fed back for position control, based on (5) and (6), the state vector is

$$\mathbf{x}(t) = \begin{bmatrix} z_M & z_S & \dot{z}_M & \dot{z}_S \end{bmatrix}^\top. \tag{23}$$

In this case the controller can be dimensioned with respect to the coefficients m_M, c and d. Further elements within the state vector are possible to compensate for the transfer function of the power electronics [11].

If the translation of the magnet is neglected, the system state depends only on the slider dynamics (6), thus the reduced state vector consists of z_S and $\dot{z}_S$. This configuration corresponds to a standard AMG. It is possible to achieve stable levitation by an ES-HAMG with a standard AMG controller. In this case, the actuating force F_M is controlled independent from the translation of the magnet.

4.2 Pole Placement

Based on [14, pp. 696-699], it is possible to freely choose all zeros and poles of a closed loop system as follows. This procedure works for both the full and the reduced state vector (section 4.1). The following equations are based on [11].

The basic state space equations are

$$\dot{\mathbf{x}}(t) = \mathbf{A}\,\mathbf{x}(t) + \mathbf{b}\,u(t), \tag{24}$$

$$y(t) = \mathbf{c}^\top \mathbf{x}(t). \tag{25}$$

The actuating variable $u(t)$ is

$$u(t) = u_{r,SS}(t) + u_{r,PI}(t) = \mathbf{r}^\top \mathbf{x}(t) + k_p\,\dot{e}(t) + k_i\,e(t), \tag{26}$$

where k_p and k_i are the PI controller gains, the control error is

$$\dot{e}(t) = w(t) - y(t). \tag{27}$$

The PI controller gains are additional parameters to place the system poles, thus it should be described in state space notation. With (25) and (27) we can extend (24) to

$$\underbrace{\begin{bmatrix} \dot{\mathbf{x}}(t) \\ \cdots \\ \dot{e}(t) \end{bmatrix}}_{\dot{\mathbf{x}}_\mathrm{e}(t)} = \underbrace{\begin{bmatrix} \mathbf{A} & \vdots & \mathbf{0} \\ \cdots & \cdots & \cdots \\ -\mathbf{c}^\top & \vdots & 0 \end{bmatrix}}_{\mathbf{A}_\mathrm{e}} \underbrace{\begin{bmatrix} \mathbf{x}(t) \\ \cdots \\ e(t) \end{bmatrix}}_{\mathbf{x}_\mathrm{e}(t)} + \underbrace{\begin{bmatrix} \mathbf{b} \\ \cdots \\ 0 \end{bmatrix}}_{\mathbf{b}_\mathrm{e}} u(t) + \begin{bmatrix} \mathbf{0} \\ \cdots \\ w(t) \end{bmatrix}, \tag{28}$$

$$y(t) = \mathbf{c}_\mathrm{e}^\top \mathbf{x}_\mathrm{e}(t) = \begin{bmatrix} \mathbf{c}^\top & \vdots & 0 \end{bmatrix} \mathbf{x}_\mathrm{e}(t). \tag{29}$$

With (26) in (28) we can replace $\mathrm{u}(t)$ which then depends on $\mathbf{x}(t)$ and $\mathrm{w}(t)$, thus the extended state space equation can be written as

$$\dot{\mathbf{x}}_e(t) = \mathbf{A}_{\mathrm{SS,PI}}\,\mathbf{x}_\mathrm{e}(t) + \mathbf{b}_{\mathrm{SS,PI}}\,w(t) \tag{30}$$

where (29) is still the output equation. From (30) we get the control transfer function

$$\mathrm{G}_\mathrm{CTF}(s) = \mathbf{c}_\mathrm{e}^\top \left(s\mathbf{I} - \mathbf{A}_{\mathrm{SS,PI}}\right)^{-1} \mathbf{b}_{\mathrm{SS,PI}}. \tag{31}$$

The number of poles and zeros depends on the number of elements in the chosen state vector (section 4.1). In case we neglect the translation of the magnet and do not compensate for the power electronics, the control transfer function is

$$G_{\mathrm{CTF,red}}(s) = \frac{k_i + k_p s}{k_i + k_p s - k_{zs} s + (d_S - k_{zsd}) s^2 + m_S s^3}. \tag{32}$$

It contains only the mechanical parameters of the slider and additional control parameters. The PI controller has the gain factors k_p and k_i, k_{zs} and k_{zsd} denote the state feedback. These four control parameters have to be set to place one zero and three poles by equating the coefficients. As $G_{\mathrm{CTF,red}}$ does not depend on the mechanical parameters of the magnet, the oscillation of the magnets mass leads to disturbances as the nonlinear compensation of the magnetic force is not instantaneous. Nevertheless, this control concept works well on the sample ES-HAMG as examined experimentally in section5.

The control transfer function of the full state (23) leads to a long expression for the control transfer function which also depends on c, d and m_M. One zero and five poles can be placed with the control parameters.

5 Experimental Validation

A test bench to carry out experiments with ES-HAMG is described in section 5.1. The power dissipation of the test configuration is measured in 5.2 while the ES-HAMG operates. The impact of the elastic suspension on positioning uncertainty is measured in section 5.3. All experiments are carried out with a PI state space controller with a reduced state vector (section 4).

5.1 ES-HAMG Test Bench

A linear test bench (Figure 9) has been presented in [2] to carry out experiments on positioning performance and power dissipation of ES-HAMG. It consists of a stage, which is linearly guided

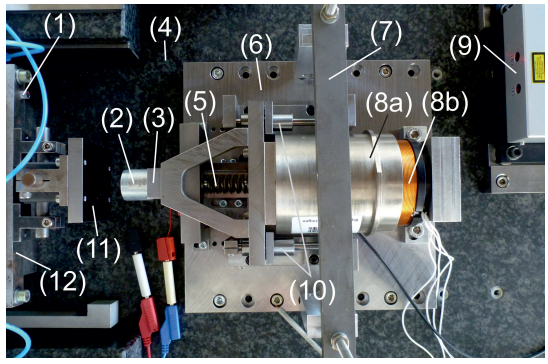

Figure 9: Top view of ES-HAMG test bench [2]

by a ball guidance (10) to allow linear motion z_M of the hybrid magnet (2). The replaceable spring with constant c (5) is connected to the movable stage and the ground plate (6). The damping d is realized by a voice coil which consists of the field assembly (8a) and the coil assembly (8b). It is operated in passive mode by connecting ohmic resistances to its clamps, making use of its counter

electromotive force. A capacitive sensor determines the position of the sensor target (3) and thus the position z_M of the hybrid magnet (2).

A linear slider, which carries the armature plate (11), is guided by aerostatic bearings. Its position z_S is measured with a mirror (1) and a laser interferometer (9). The slider is actuated to apply different load forces. Table 1 shows a brief overview on the test bench.

Moving mass (slider)	m_S	$7.92\,\mathrm{kg}$
Damping (slider)	d_S	$7.9\,\frac{\mathrm{Ns}}{\mathrm{m}}$
Moving mass (magnet)	m_M	$2.9\,\mathrm{kg}$
Adjustable damping (magnet)	d	$50 \leq 500\,\frac{\mathrm{Ns}}{\mathrm{m}}$
ES-HAMG spring constant	c	$42\,\frac{\mathrm{N}}{\mathrm{m}}$
Zero power contact force (magnet)	$F_M(0,0)$	$45\,\mathrm{N}$

Table 1: Overall technical data of the test bench

5.2 Power Dissipation at varying load

To measure the power dissipation at varying load, the load force F_L is varied within 120 seconds from 6 N to 12 N and back to 6 N (steady state). The controller keeps the slider at a constant position z_S. The power dissipation P_d is computed from the measured current signal and the ohmic resistance of the coil according to (9). Figure 10 shows P_d during increasing, figure 11 during decreasing load for three different HAMG configurations.

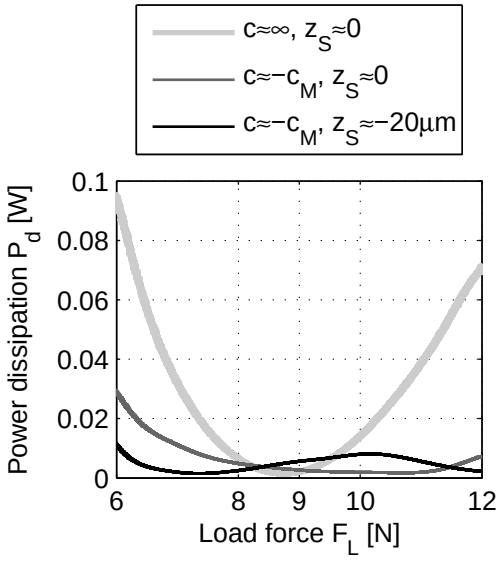

Figure 10: Experimental power dissipation with increasing load force [2]

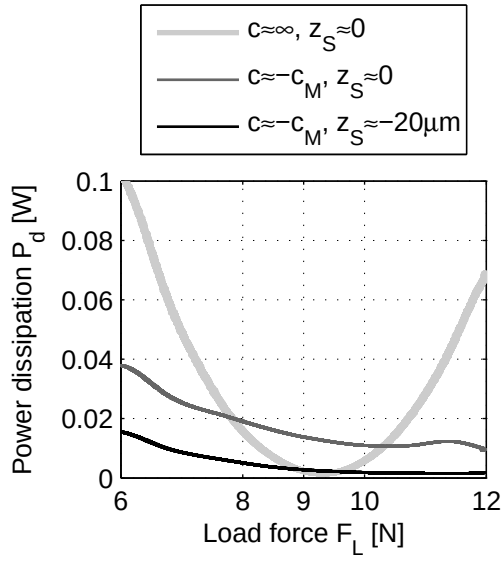

Figure 11: Experimental power dissipation with decreasing load force [2]

In figure 10, all configurations largely match the theoretical considerations in figures 6 and 7. Zero Power cannot be achieved in practice, the minimum value is $P_{d,min} = 0,0011W$, thus at normal

operation it is only a small fraction of the entire dissipation.

At decreasing load (Figure 11), the behaviour differs from increasing load. For the HAMG ($c \approx \infty$), the minimum value $P_{d,min}$ occurs at a slightly higher load force than in figure 10. As the working gap δ is kept konstant in this configuration, the reason might be magnetic hysteresis. Both ES-HAMG configurations ($c = -c_M$) show significant differences between increasing and decreasing load. The reason is mechanical hysteresis of about $z_{M,hyst} \approx 20\,\mu$m that has been measured, thus the experiment does not comply with (21) exactly. One can see, that the sliders position $z_S = -20\,\mu$m is beneficial as P_d osculates minimum power two times at increasing and one time at decreasing load. The overall power dissipation within the load range is $P_{d,max} = 14\,$mW and $P_{d,mean} = 4.7\,$mW. The overall power dissipation for the HAMG is more than six times larger for both values.

5.3 Positioning Error

Generally, there are many factors of influence on the positioning uncertainty. In AMG, the behaviour of the plant changes at a varying working gap δ, as the inductance and the current to force factor varies. Depending on the power electronics, this has more or less impact on the actuation. The working gap in ES-HAMG differs from HAMG, thus different positioning uncertainties can be expected. The control error of the test bench has been measured for several working points at a constant load force and constant reference input.

No.	Configuration	F_L [N]	δ [μm]	σ_{z_S} [nm]	$z_{S,peak}$ [nm]
1	HAMG/ES-HAMG	9	291	9.5	75
2	HAMG	6.25	291	9.6	68
3	ES-HAMG	6.25	406	6.9	51
4	HAMG	10.85	291	13.8	95
5	ES-HAMG	10.85	221	14.5	99

Table 2: Positioning uncertainty at increasing load force

Table 2 lists the measured positioning uncertainties. The HAMG and ES-HAMG configuration showed approximately the same position standard deviations σ_{z_S} and peak to peak values $z_{S,peak}$ (No. 1). This is the only point of operation, where both configurations had the same working gap. This implies, that the elastic suspension does not affect the positioning uncertainty for a given point of operation of the magnet. At $F_L = 6.25\,$N (No. 2,3), the working gap of the ES-HAMG is larger

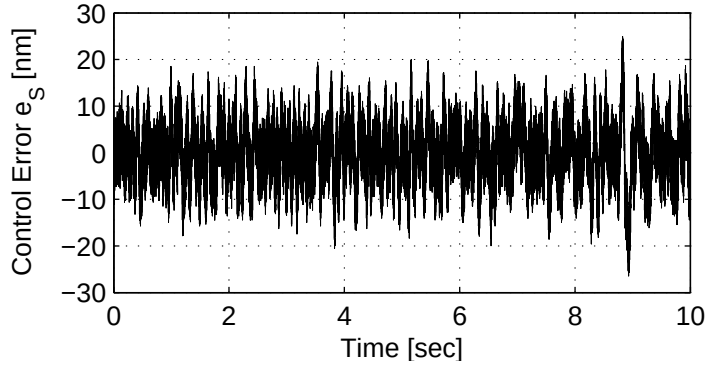

Figure 12: Control error for ES-HAMG configuration according to no. 3 in table 2

and the ES-HAMG has a better positioning uncertainty. Figure 12 shows the control error for ten seconds of the associated measurement. At higher loads (no. 4,5), the HAMG has a larger working gap, thus is beneficial this time.

5.4 Force Step Response

In theory, the elastic suspension has no effect on the sliders motion with PI state space control and a reduced state vector (4). Practically the actuation variable is disturbed by the magnets motion. A force step is measured to examine the impact of the elastic suspension.

Figure 13 shows both positions of the slider and the magnet after a forcestep at $t = 0.1\,\text{sec}$. The slider is dislocated due to the force step, the HAMG ($c \approx \infty$) is dislocated even more than the

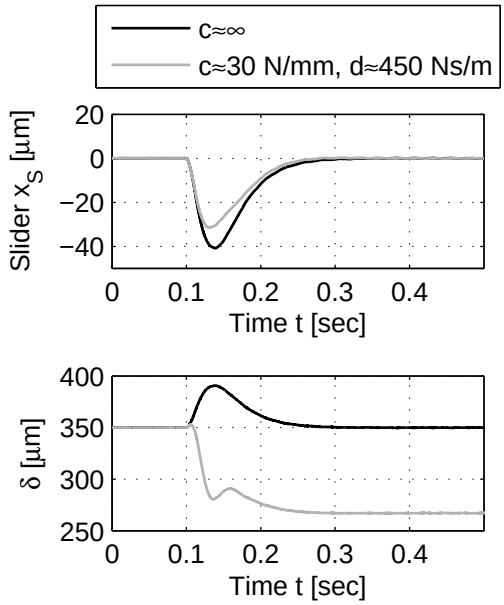

Figure 13: Position x_S and working gap δ at a load force step $\Delta F_L \approx 2.75\,\text{N}$ at $t = 0.1\,\text{sec}$

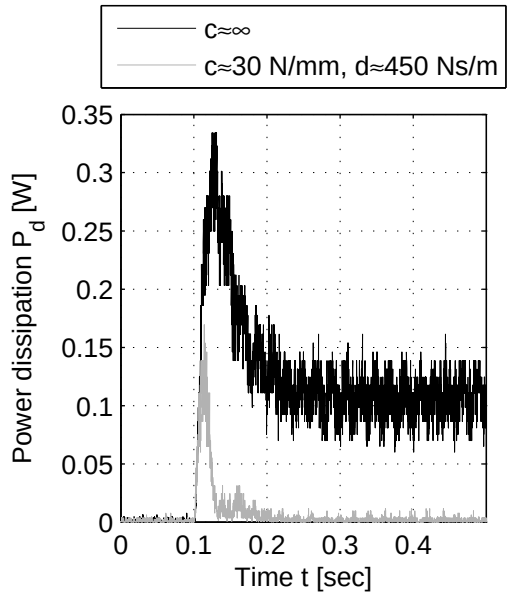

Figure 14: Power dissipation P_d at a load force step $\Delta F_L \approx 2.75\,\text{N}$ at $t = 0.1\,\text{sec}$

ES-HAMG ($c \approx 30$). The HAMG increases its air gap according to the sliders translation x_S. The ES-HAMG increases its working gap at first, at $t = 0.011\,\text{sec}$, δ falls below its initial value and engages its final offset of $83\mu\text{m}$. A changing working gap causes a disturbance force the controller can only compensate delayed. According to (17), the decreasing air gap of the ES-HAMG causes a disturbance force which supports the controller thus the slider is dislocated less.

Figure 14 shows the Power dissipation (raw data) during the load force step described in figure 13. Initially, both configurations approach zero power. When the step occurs, the power dissipation raises to its maximum value ($P_{d,c\infty} \approx 0.33\,\text{W}$, $P_{d,c30} \approx 0.17\,\text{W}$). In steady state ($t > 0.3\,\text{sec}$), the ES-HAMG approaches its initial power dissipation where the HAMG has an offset of $P_{d,c\infty} \approx 0.1\,\text{W}$. The variation of the power dissipation is significantly lower at lower absolute values. Beside the steady state, the ES-HAMG also reduces energy consumtption for load steps depending on the dynamics of the magnet.

6 Conclusion

ES-HAMG devices may reduce thermal dissipation in steady state about 90% theoretically, savings around 80% have been validated experimentally. Magnetic hysteresis and hysteresis in motion limit the achievable value. However, the working gap should be selected carefully to gain full benefit of the elastic support.

Regarding its controller design, ES-HAMG has been succesfully operated with a standard HAMG Controller. The working gap has been measured with an additional capacitive sensor to compensate for magnetic nonlinearities.

The positioning uncertainty does not suffer from the elastic support in the test configuration. ES-HAMG can have a superiour control error compared to HAMG and vice versa, depending on the actual load.

The test bench exceeds maintainable dimensions for commercial application, thus further research has to be made to manufacture smaller devices.

This contribution was funded by the german collaborative research center (SFB) 622.

References

[1] Layton Carter Hale. *Principles and Techniques for Designing Precision Machines*. PhD thesis, Massachusetts Institute of Technology, 1999.

[2] Mirko Büchsenschütz and Thomas Sattel. A hybrid active magnetic guidance concept with low heat production for high precision machines. *Proc. 13th Int. Conf. on New Actuators*, pages 221–224, 2012.

[3] Thomas Sattel, Ralf Volkert, Steffen Hesse, and Christoph Schäffel. Planar magnetic drives and bearings for multi-axis nanopositioning machines with large travel ranges. *Proc. 12th Int. Conf. on New Actuators*, 1:276–279, 2010.

[4] Sergej Kovalev. *Magnetisch geführter Mehrkoordinaten Präzisionsantrieb*. PhD thesis, TU-Ilmenau, 2001.

[5] Alexander Molenaar. *A novel Planar Magnetic Bearing and Motor Configuration applied in a Positioning Stage*. PhD thesis, TU Delft, 2000.

[6] Toshiyuki Ueno and Toshiro Higuchi. Combination of magnetostrictive/ piezoelectric materials composite and electromagnet for zero power levitation. *Proc. 10th Int. Symposium On Magnetic Bearings*, 2006.

[7] Koichi Oka, Noriaki Ninomiya, Li Chen, and Yusuke Fujiwara. Magnetic suspension system with variable flux path mechanism using rotary actuator. *Proc. 10th Int. Symposium on Magnetic Bearing*, 2006.

[8] Takeshi Morita. A miniaturized levitation system with motion control using a piezoelectric actuator. *IEEE TRANSACTIONS ON CONTROL SYSTEMS TECHNOLOGY*, 10:666 – 670, 2002.

[9] Marcus Herrmann and Heinz Ulbrich. Studies on coil-less reluctance force actuators. *Proc. 10th Int. Symposium On Magnetic Bearings*, 2006.

[10] Md Emdadul Hoque, Masaya Takasaki, Yuji Ishino, Hirohisa Suzuki, and Takeshi Mizuno. An active micro vibration isolator with zero-power controlled magnetic suspension technology. *JSME Int. Journal*, 49:719–726, 2006.

[11] Ralf Volkert, Mirko Büchsenschütz, and Thomas Sattel. Design of a nanometre-precision air gap control for planar magnetic bearing actuators. *Proc. 10th EUSPEN Int. Conf.*, 1:312–315, 2010. Delft.

[12] Gerhard Schweitzer, Alfons Traxler, and Hannes Bleuler. *Magnetlager - Grundlagen, Eigenschaften und Anwendungen berührungsfreier elektromagnetischer Lager*. Springer Verlag, 1993.

[13] Eberhard Kallenbach, Rüdiger Eick, Peer Quendt, Tom Ströhla, Karsten Feindt, and Matthias Kallenbach. *Elektromagnete: Grundlagen, Berechnung, Entwurf und Anwendung*. Teubner Verlag, 2nd edition, 2003.

[14] Holger Lutz and Wolfgang Wendt. *Taschenbuch der Regelungstechnik*. Wissenschaftlicher Verlag Harri Deutsch, Frankfurt am Main, 8th edition, 2010.